Chinese Chemical Letters 36 (2025) 110444

Contents lists available at ScienceDirect

Chinese Chemical Letters

journal homepage: www.elsevier.com/locate/cclet

Efficient propane dehydrogenation catalyzed by Ru nanoparticles anchored on a porous nitrogen-doped carbon matrix

Tianyi Yang[a], Fangxi Su[a], Dehuan Shi[b], Shenghong Zhong[b], Yalin Guo[a], Zhaohui Liu[a,*], Jianfeng Huang[a,*]

[a] State Key Laboratory of Coal Mine Disaster Dynamics and Control, Institute of Advanced Interdisciplinary Studies, School of Chemistry and Chemical Engineering, Chongqing University, Chongqing 400044, China
[b] Key Laboratory of Advanced Materials Technologies, International (HongKong Macao and Taiwan) Joint Laboratory on Advanced Materials Technologies, College of Materials Science and Engineering, Fuzhou University, Fuzhou 350108, China

ARTICLE INFO

Article history:
Received 11 May 2024
Revised 9 September 2024
Accepted 10 September 2024
Available online 11 September 2024

Keywords:
Propane dehydrogenation
Ru nanoparticles
Porous carbon matrix
Ru@NC
Electronic interaction

ABSTRACT

Propane dehydrogenation (PDH) is a vital industrial process for producing propene, utilizing primarily Cr-based or Pt-based catalysts. These catalysts often suffer from challenges such as the toxicity of Cr, the high costs of noble metals like Pt, and deactivation issues due to sintering or coke formation at elevated temperatures. We introduce an exceptional Ru-based catalyst, Ru nanoparticles anchored on a nitrogen-doped carbon matrix (Ru@NC), which achieves a propane conversion rate of 32.2% and a propene selectivity of 93.1% at 550 °C, with minimal coke deposition and a low deactivation rate of 0.0065 h^{-1}. Characterizations using techniques like TEM and XPS, along with carefully-designed controlled experiments, reveal that the notable performance of Ru@NC stems from the modified electronic state of Ru by nitrogen dopant and the microporous nature of the matrix, positioning it as a top contender among state-of-the-art PDH catalysts.

Propene, a crucial industrial building block, can be produced through a combination of steam cracking of naphtha, fluid catalytic cracking, and propane dehydrogenation (PDH). While steam cracking remains the dominant source of propene globally, PDH is gaining importance and popularity as a stand-alone process due to the availability of propane from natural gas processing and shale gas production. Presently, many commercial PDH processes employ chromium (Cr)-based or platinum (Pt)-based catalysts [1–9], although some processes, such as K-PRO TECHNOLOGY, utilize proprietary catalysts claimed to be non-Pt/Cr, with the exact composition remaining publicly undisclosed. Nevertheless, traditional technologies that use Cr and Pt catalysts are beset by challenges such as the toxicity associated with Cr-compounds, the high cost of noble metal Pt-based catalysts, or the utilization of environmentally detrimental chlorine for the redispersion of noble Pt-catalysts to prevent sintering.

Moreover, PDH is an endothermic process that necessitates high reaction temperatures. The elevated temperature readily induces C–C bond cleavage and concurrent coke formation [10–14]. For instance, Cr-based catalysts exhibit relatively low propene selectivity and confront accelerated catalyst deactivation due to severe coke deposition. This mandates periodic catalyst regeneration every 12 min, resulting in the emission of carbon dioxide and raising environmental concerns [4,5]. In light of these environmental and economic imperatives, there is a pressing need to explore cost-effective and eco-friendly PDH catalysts with desired propene selectivity, a pursuit deemed crucial in both industrial and academic realms.

In recent years, various strategies have been developed to address this objective [15–23]. For instance, the creation of Pt-based bimetallic catalysts with isolated Pt sites has shown enhanced propene selectivity and reduced coke formation rates compared to Pt ensembles of larger sizes [17–19]. This approach not only effectively lowers the cost of the catalysts through the incorporation of a secondary metal but also adjusts the electronic state and surface structure of the active species, thereby enhancing the performance of PDH catalysts. Concurrently, Ru-based catalysts, recognized for their favorable activity in C–H bond activation, have been extensively explored as alternatives to Pt-based catalysts due to their relatively lower cost. Yang *et al.* observed that the introduction of phosphorus (P) elements resulted in electron-deficient Ru sites in Ru-P catalysts, significantly contributing to PDH activity [24]. Additionally, Ma *et al.* demonstrated that an increase in P content

* Corresponding authors.
E-mail addresses: zhaohui.liu@cqu.edu.cn (Z. Liu), jianfeng.huang@cqu.edu.cn (J. Huang).

https://doi.org/10.1016/j.cclet.2024.110444
1001-8417/

in Ru-P catalysts exhibited a linear promotion of propene selectivity [25]. More recently, Zhou *et al*. created a highly selective catalyst comprising single-atom Ru anchored on nitrogen-doped carbon (Ru_1/NC). Their findings revealed that inner-shell N inhibited propane cracking, while outer-shell N facilitated high propene selectivity [26]. Building upon previous research, we get inspired that customizing the electronic state and surface structure of Ru sites presents a promising avenue for developing efficient Ru-based PDH catalysts.

Herein, we report a facile preparation of a Ru-based PDH catalyst, consisting of Ru nanoparticles anchored on a nitrogen-doped carbon matrix (Ru@NC), through a simple and widely-used pyrolysis method [27], involving a Ru precursor incorporated into ZIF-8 (Ru@ZIF-8). The Ru@NC catalyst exhibits exceptional PDH performance, achieving ~32.2% propane conversion and ~93.1% propene selectivity at 550 °C, with a feed composition of $C_3H_8/N_2 = 1/19$ and a weight hourly space velocity (WHSV) of 1.2 h^{-1}. Furthermore, it maintains this high selectivity of ~93% for over 50 h. Through a combination of TEM, XPS characterizations, and carefully designed control experiments, we elucidate that the porous NC-confined electron-deficient Ru sites are responsible for the enhanced activity and stability in the PDH process.

The Ru@NC catalyst was synthesized from a Ru@ZIF-8 precursor using a straightforward pyrolysis method. As depicted schematically in Fig. 1a, $Ru(acac)_3$ was initially co-precipitated in the synthetic solution of ZIF-8 to prepare Ru@ZIF-8. The Ru precursor, utilizing coordination chemistry similar to that of the Zn precursor, was introduced *in-situ* into the ZIF-8 by coordinating with 2-methylimidazole. Subsequently, the resultant Ru@ZIF-8 powder was heated at 1000 °C for 2 h under an N_2 atmosphere. This pyrolysis process led to the transformation of ZIF-8 into NC, the evaporation of Zn, and the anchoring of Ru, ultimately resulting in the formation of the Ru@NC product. The synthetic details can be found in Supporting information.

The obtained Ru@ZIF-8 particles exhibit the same sodalite-like crystal structure and rhombic dodecahedron shape (~600 nm in edge length) as ZIF-8, as evidenced by powder X-ray diffraction (XRD, Fig. S1 in Supporting information) and transmission electron microscopy (TEM, Fig. S2 in Supporting information), respectively. Energy-dispersive X-ray spectroscopy (EDX) elemental mapping demonstrates the successful incorporation of the Ru element into ZIF-8 (Fig. S2). Following calcination, the resulting Ru@NC catalyst manifests a distinctly different structure and morphology. High-angle annular dark-field scanning transmission electron microscopy (HAADF-STEM) images clearly depict tiny nanoparticles with brighter contrasts uniformly dispersed on a porous substrate of a dimmer contrast (Figs. 1b and c). Visually, the substrate comprises irregularly shaped particles forming a network, derived from the ZIF-8 particles. The nanoparticles have a mean size of 6.69 ± 0.97 nm, as indicated by the size statistical analysis in Fig. 1d. The high-resolution TEM image of a nanoparticle reveals a lattice spacing of 0.23 nm, corresponding to the (111) facets of face-centered cubic (fcc) Ru (Fig. 1e). In agreement with this structure information, the XRD pattern shows a broad (111) diffraction peak for these small Ru nanoparticles (Fig. S1). The HAADF-STEM image and its corresponding EDX elemental mapping of Ru@NC (Fig. 1c) confirm a uniform distribution of C, N elements, and Ru ensembles across the substrate. ICP-OES and EDS analyses reported that the Ru mass loadings are 0.37 wt% and 0.41 wt%, respectively, while no Zn content was detected. Additionally, CHN elemental analysis shows that the N content is 4.1 wt%.

To investigate the electronic interactions between Ru and N, we conducted X-ray photoelectron spectroscopy (XPS) tests on Ru@NC and compared the results with those of Ru/C and NC (Figs. 2a and b). The XPS full spectrum and high-resolution C 1s spectrum used for standard calibration are provided in Fig. S3 (Supporting information). The Ru 3p spectra of Ru@NC exhibit two distinguishable doublets with $3p_{3/2}$ peaks at binding energies of 461.9 eV and 465.6 eV, corresponding to Ru^0 and Ru^{3+}, respectively (Fig. 2a) [26–28]. The N 1s spectra of NC can be deconvoluted into three characteristic peaks at binding energies of 402.1 eV, 399.9 eV, and 397.4 eV, assigned to graphitic N, pyrrolic N, and pyridinic N, respectively (Fig. 2b) [29,30]. A noticeable positive shift (0.70 eV) in the Ru 3p binding energies of Ru@NC relative to Ru/C suggests an

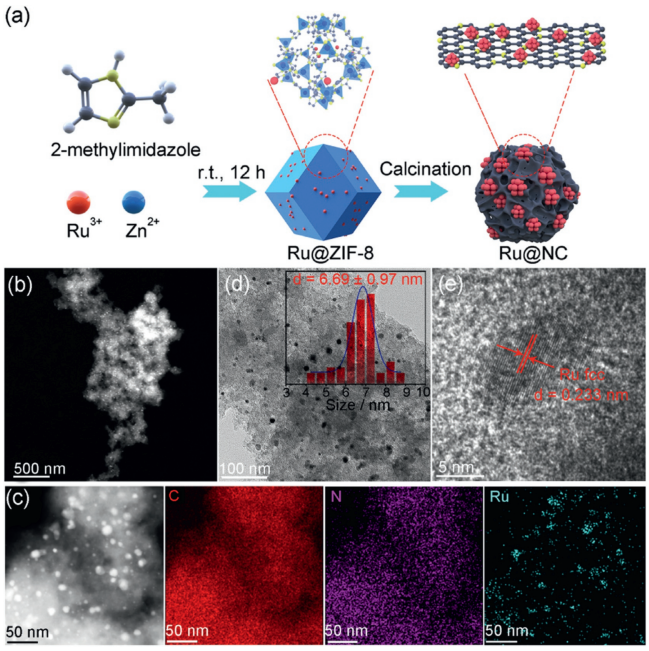

Fig. 1. (a) Schematic illustration of the synthesis and (b-e) TEM characterizations of Ru@NC, including low-magnification HAADF-STEM image (b), high-magnification HAADF-STEM image with corresponding EDX elemental mapping for C (red), N (purple), and Ru (blue) (c), TEM image (d), and high-resolution TEM image (e). The inset histogram in (d) displays the statistical size distribution of the Ru nanoparticles, based on analysis of over 50 particles.

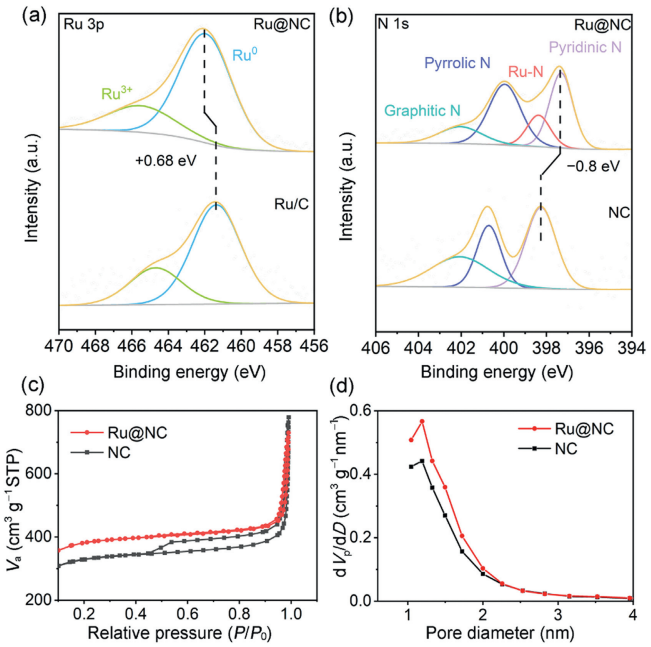

Fig. 2. (a) Ru 3p and (b) N 1s XPS spectra of Ru@NC in comparison with Ru/C and NC, respectively. (c) N_2 adsorption/desorption isotherms and (d) pore size distribution for Ru@NC and NC.

electron loss from Ru induced by the presence of N. Correspondingly, taking the pyridinic N peak as an example, the binding energy for Ru@NC undergoes a negative shift (0.8 eV) compared to NC. These findings provide evidence of a robust electronic interaction between Ru and N, inducing charge transfer from Ru to N and creating electron-deficient Ru sites. Notably, when compared with NC, an additional peak at 398.3 eV emerges in the N 1s spectra of Ru@NC, which is attributed to the Ru-N bond [26], further confirming the strong electronic interaction between Ru and N. Additionally, we conducted XPS analysis on other control samples including Ru_{pre}/NC_{pre} and $Ru@NC_{pre}$, alongside Ru@NC, Ru/C, and NC. Definitions and synthetic details of these samples are provided in the experimental section of Supporting information and Fig. S4 (Supporting information), with corresponding TEM images shown in Figs. S5-S8 (Supporting information), Ru mass loadings in Fig. S9 (Supporting information), and XPS spectra in Fig. S10 (Supporting information). Interestingly, unlike Ru_{pre}/NC_{pre}, $Ru@NC_{pre}$ and Ru@NC are the two Ru-containing samples that exhibit a distinct negative shift in the N 1s binding energy and a positive shift in the Ru 3p binding energy relative to NC and Ru/C, respectively. This result clearly demonstrates the presence of electronic interactions between Ru and N in the $Ru@NC_{pre}$ and Ru@NC samples, and also suggests that the high-temperature calcination process is pivotal for establishing such robust electronic interactions between the metallic nanoparticles and the substrate.

Considering the porous nature of the NC support, we also examine the textural properties of Ru@NC and NC by N_2 adsorption-desorption isotherms (Figs. 2c and d). The Brunauer–Emmett–Teller (BET) method was employed to determine the surface areas of the samples, revealing exceptionally high values of 1046 m^2/g and 1203 m^2/g for NC and Ru@NC, respectively. Moreover, the Barrett-Joyner-Halenda (BJH) method was utilized to analyze the N_2 adsorption branches in the isotherms, indicating that the pore size of both NC and Ru@NC is approximately 1.3 nm. The significant surface area and microporous structure of the Ru@NC catalyst are expected to facilitate the mass diffusion of reactants and products during the PDH reaction, thereby improving the catalytic performance. Furthermore, the mesopores largely disappear in Ru@NC (Fig. 2c), indicating the embedment of Ru nanoparticles within the mesopores. This structure is likely to impede particle mobility, reducing sintering and thereby enhancing the catalyst's stability.

The catalytic performance of Ru@NC catalyst for the PDH reaction was then evaluated in a fixed-bed quartz reactor. At a WHSV for propane of 1.2 h^{-1}, the Ru@NC catalyst exhibited an increasing trend in propane conversions, ranging from 12.1% to 57.0%, as the temperature rose from 500 °C to 600 °C, while the propene selectivity decreased from 95.9% to 73.7% (Fig. 3a). Given the endothermic nature of the PDH reaction [30–32], it is imperative to maintain a sufficiently high reaction temperature to drive the process. However, elevated temperatures commonly trigger side cracking reactions, adversely affecting propene formation. Impressively, the Ru@NC catalyst achieved a remarkably high propane conversion rate of 32.2% at 550 °C, alongside a high propene selectivity of 93.1%, while also exhibiting minimal coke formation. By taking into account the Ru molar loading, the turnover frequency (TOF) for propene formation has been calculated to reach 228 $mol_{propene}$ mol_{Ru}^{-1} h^{-1}. Catalyst stability constitutes another vital parameter for industrial applications. Therefore, we investigated the longevity of Ru@NC for the PDH reaction. As presented in Fig. 3b, the propane conversion exhibited a slight decrease from 32.2% to 25.6% after 50 h on stream at 550 °C, while the propene selectivity remained high at ~93%. The deactivation rate constant (k_d), calculated based on a first-order deactivation model (see calculation details in Supporting information), was found to be only 0.0065 h^{-1}, comparable to that of the most stable Ru-based PDH catalyst reported to date, *i.e.*, Ru_1/NC (0.0048 h^{-1}) [26]. We

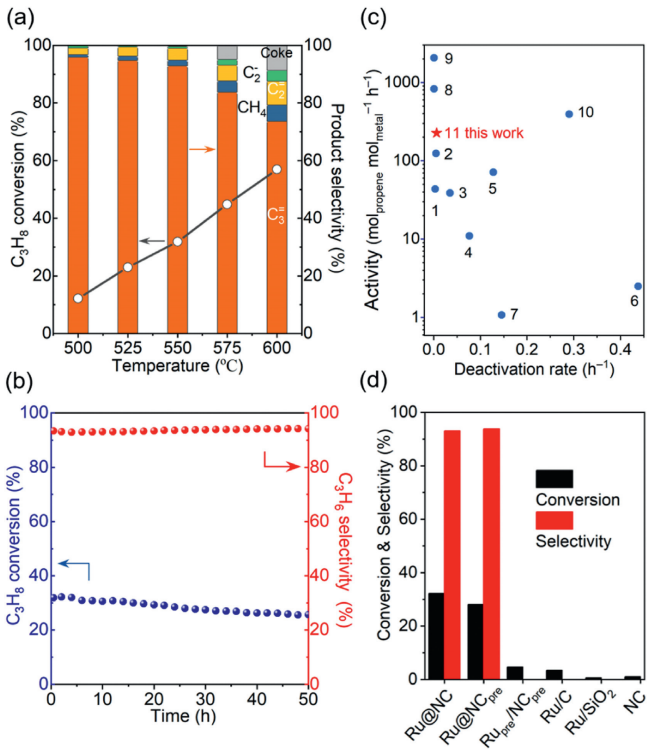

Fig. 3. (a) Propane conversion and product selectivity as a function of the reaction temperature over Ru@NC. (b) Stability test of Ru@NC for PDH reaction. Reaction conditions: atmospheric pressure, 550 °C, $WHSV_{C_3H_8} = 1.2\ h^{-1}$, $C_3H_8:N_2 = 19:1$. (c) Comparison of Ru@NC's performance, in terms of activity and deactivation rate, with several reported state-of-the-art Pt-, Ru-, and Cr-based catalysts (1–2: Ru_1/NC, 3: RuNP/NC, 4: $Ru/YZrO_x$, 5: Ru-P/SiO_2, 6: CrO_x/Al_2O_3, 7: $PdZn/Al_2O_3$, 8: PtZn/Silicalite-1, 9: $PtCu/Al_2O_3$, 10: $PtSn/Al_2O_3$, 11: Ru@NC) refer to Table S1 for additional information). (d) Propane conversion and propene selectivity over Ru@NC, $Ru@NC_{pre}$, Ru_{pre}/NC_{pre}, Ru/C, Ru/SiO_2 and NC support.

attribute such exceptional stability of this easily prepared Ru@NC catalyst to the confinement and hindrance effects of the porous NC support, which inhibit the transportation and thus sintering of Ru nanoparticles (Fig. S11 in Supporting information). The exceptional performance of Ru@NC positions this catalyst as one of the top contenders among PDH catalysts (Fig. 3c and Table S1 in Supporting information). When comparing the propane conversion and propene selectivity of Ru@NC, $Ru@NC_{pre}$, Ru_{pre}/NC_{pre}, Ru/C, Ru/SiO_2, and NC (Fig. 3d), among the first five Ru-based samples with similar Ru nanoparticle sizes and loadings (Figs. S6-S9 and S12 in Supporting information), Ru@NC and $Ru@NC_{pre}$, both exhibiting Ru-N electronic interaction as revealed by the XPS tests, are unequivocally superior to the other control samples. This result further underscores the significance of Ru-N electronic interaction during the PDH process.

Finally, kinetic experiments were conducted to investigate further the Ru@NC-catalyzed PDH process at relatively low propane conversions (<10%) [7]. As depicted in Fig. 4a, the Ru@NC catalyst displays a propane reaction order of 0.58 and an H_2 reaction order of −0.11, suggesting that propane activation is the rate-determining step in the Ru-catalyzed PDH process. The reaction order value (−0.11) close to zero for H_2 also indicates that desorption of the side product H_2 from Ru@NC occurs rapidly, with negligible inhibitory effects on the overall reaction pathway. Similar to previously reported Zn-based catalysts, the interaction between Ru sites and H_2 is relatively weak [33]. Furthermore, the activation energy of propene formation was determined based on the Arrhenius equation (please see Supporting information for details). As illustrated in Fig. 4b, both Ru@NC and $Ru@NC_{pre}$ exhibit similar ap-

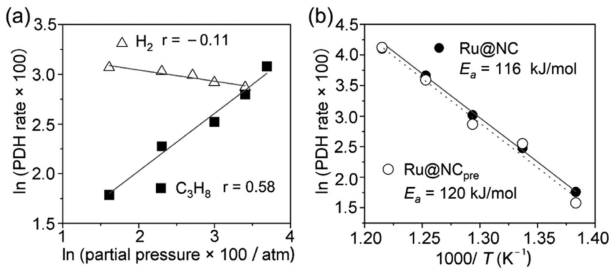

Fig. 4. (a) Dependence of PDH rates on propane and H_2 partial pressure catalyzed by Ru@NC at 500 °C. (b) Arrhenius plots of Ru@NC and Ru@NC$_{pre}$ catalysts. Reactions were carried out at 450, 475, 500, 525, 550 °C, and the conversion of propane in each reaction was kept <10% by using a high $WHSV_{C_3H_8}$. The PDH rates has the unit $mmol_{C_3H_6}$ g_{cat}^{-1} min^{-1}.

parent activation energy (~120 kJ/mol), suggesting the presence of the same active structure, attributed to the electronic interaction between Ru and N.

In conclusion, we have developed a catalyst consisting of Ru nanoparticles immobilized in a porous nitrogen-doped carbon matrix (Ru@NC), synthesized *via* a straightforward pyrolysis technique using Ru@ZIF-8 as the precursor. The electronic interaction between Ru and N alters the electronic state of Ru, endowing the catalyst with exceptional performance in the PDH reaction. Impressively, it achieved a propane conversion rate of 32.2% and a propene selectivity of 93.1% at 550 °C, while also showing minimal coke deposition and a low deactivation rate (0.0065 h^{-1}). The simplicity of the synthesis and the robust structure render the Ru@NC catalyst a highly promising candidate for industrial PDH processes. Moreover, the fundamental insights provided by this research pave the way for the design of superior PDH catalysts through the electronic modulation of metal active sites by non-metal elements.

Declaration of competing interest

The authors declare that they have no known competing financial interests or personal relationships that could have appeared to influence the work reported in this paper.

CRediT authorship contribution statement

Tianyi Yang: Writing – original draft, Formal analysis, Data curation, Conceptualization. **Fangxi Su:** Data curation, Conceptualization. **Dehuan Shi:** Data curation. **Shenghong Zhong:** Writing – review & editing, Formal analysis. **Yalin Guo:** Writing – original draft, Funding acquisition, Formal analysis, Data curation. **Zhaohui Liu:** Writing – review & editing, Writing – original draft, Supervision, Funding acquisition, Formal analysis, Data curation, Conceptualization. **Jianfeng Huang:** Writing – review & editing, Supervision, Project administration, Funding acquisition, Formal analysis, Conceptualization.

Acknowledgments

This work was supported by the National Key Research and Development Project of China (No. 2022YFE0113800), the National Natural Science Foundation of China (No. 22102013), Natural Science Foundation of Chongqing (No. cstc2021jcyj-msxmX0945), Venture and Innovation Support Program for Chongqing Overseas Returnees (No. cx2020107), Thousand Talents Program for Distinguished Young Scholars, Postdoctoral Fellowship Program of CPSF (No. GZB20230910).

Supplementary materials

Supplementary material associated with this article can be found, in the online version, at doi:10.1016/j.cclet.2024.110444.

References

[1] M. Alcantara-Rodriguez, E. Rodriguez-Castellon, A. Jimenez-Lopez, Langmuir 15 (1999) 1115–1120.
[2] J.J. Sattler, J. Ruiz-Martinez, E. Santillan-Jimenez, B.M. Weckhuysen, Chem. Rev. 114 (2014) 10613–10653.
[3] J. Gascón, C. Téllez, J. Herguido, M. Menéndez, Appl. Catal. A: Gen. 248 (2003) 105–116.
[4] S. Chen, X. Chang, G. Sun, et al., Chem. Soc. Rev. 50 (2021) 3315–3354.
[5] J. Dou, J. Funderburg, K.R. Yang, et al., ACS Catal. 13 (2023) 213–223.
[6] M. Monai, M. Gambino, S. Wannakao, B.M. Weckhuysen, Chem. Soc. Rev. 50 (2021) 11503–11529.
[7] T. Otroshchenko, G. Jiang, V.A. Kondratenko, U. Rodemerck, E.V. Kondratenko, Chem. Soc. Rev. 50 (2021) 473–527.
[8] D. Zhao, X. Tian, D.E. Doronkin, et al., Nature 599 (2021) 234–238.
[9] S. Zhao, B. Xu, L. Yu, Y. Fan, Chin. Chem. Lett. 29 (2018) 475–478.
[10] S. Chen, Z.J. Zhao, R. Mu, et al., Chem 7 (2021) 387–405.
[11] Q. Zhao, S.Y. Huang, X.X. Han, et al., Carbon 173 (2021) 364–375.
[12] Y.K. Yang, R.R. Song, X. Fan, et al., Chin. Chem. Lett. 34 (2023) 107257.
[13] J. Gong, S.X. Hou, Y. Wang, X.B. Ma, Trans. Tianjin Univ. 29 (2023) 196–208.
[14] W.Y. Bian, X.L. Shen, H. Tan, et al., Chin. Chem. Lett. 34 (2023) 107289.
[15] A.H. Motagamwala, R. Almallahi, J. Wortman, V.O. Igenegbai, S. Linic, Science 373 (2021) 217–222.
[16] L. Zeng, K. Cheng, F. Sun, et al., Science 383 (2024) 998–1004.
[17] Q. Sun, N. Wang, Q. Fan, et al., Angew. Chem. Int. Ed. 59 (2020) 19450–19459.
[18] Y. Nakaya, E. Hayashida, H. Asakura, et al., J. Am. Chem. Soc. 144 (2022) 15944–15953.
[19] H.C. Kwon, Y. Park, J.Y. Park, et al., ACS Catal. 11 (2021) 10767–10777.
[20] H. Zhu, D.H. Anjum, Q. Wang, et al., J. Catal. 320 (2014) 52–62.
[21] Y. Ma, S.J. Song, C.C. Liu, et al., Nat. Catal. 6 (2023) 506–518.
[22] W. Bian, X. Shen, H. Tan, et al., Chin. Chem. Lett. 34 (2023) 107289.
[23] R. Almallahi, J. Wortman, S. Linic, Science 383 (2024) 1325–1331.
[24] T. Yang, Y. Zhong, J. Li, et al., ACS Appl. Mater. Interfaces 13 (2021) 33045–33055.
[25] R. Ma, T. Yang, J. Gao, et al., ACS Catal. 10 (2020) 10243–10252.
[26] Y.L. Zhou, F.F. Wei, H.F. Qi, et al., Nat. Catal. 5 (2022) 1145–1156.
[27] Y.M. Tian, H. Wu, A. Hanif, et al., Chin. Chem. Lett. 34 (2023) 108056.
[28] D.J. Morgan, Surf. Interface Anal. 47 (2015) 1072–1079.
[29] X. Li, A.E. Surkus, J. Rabeah, et al., Angew. Chem. Int. Ed. 59 (2020) 15849–15854.
[30] Y. Wang, Y. Liu, W. Liu, et al., Energ. Environ. Sci. 13 (2020) 4609–4624.
[31] X.C. Li, Y.H. Liu, D.J. Zhao, et al., Trans. Tianjin Univ. 30 (2024) 90–102.
[32] J. Sattler, I.D. Gonzalez-Jimenez, A.M. Mens, et al., Chem. Commun. 49 (2013) 1518–1520.
[33] Y. Yuan, R.F. Lobo, ACS Catal. 13 (2023) 4971–4984.